Weather and Climate Extremes 37 (2022) 100470

Contents lists available at ScienceDirect

Weather and Climate Extremes

journal homepage: www.elsevier.com/locate/wace

The spatial pattern of extreme precipitation from 40 years of gauge data in the central Himalaya

Shakil Regmi [a,b,*], Bodo Bookhagen [c]

[a] Department of Forestry and Environmental Technology, South-Eastern Finland University of Applied Sciences, 50100, Mikkeli, Finland
[b] Department of Geography Didactics, Martin Luther University Halle-Wittenberg, 06120, Halle (Saale), Germany
[c] Institute of Geosciences, University of Potsdam, Karl-Liebknecht-Str. 24-25, 14476, Potsdam, Germany

ARTICLE INFO

Keywords:
Himalaya
Nepal
Indian summer monsoon
Precipitation
Extreme precipitation

ABSTRACT

The topography of the Himalaya exerts a substantial control on the spatial distribution of monsoonal rainfall, which is a vital water source for the regional economy and population. But the occurrence of short-lived and high-intensity precipitation results in socio-economic losses. This study relies on 40 years of daily data from 204 ground stations in Nepal to derive extreme precipitation thresholds, amounts, and days at the 95th percentile. We additionally determine the precipitation magnitude-frequency relation. We observe that extreme precipitation amounts follow an almost uniform band parallel to topographic contour lines in the southern Himalaya mountains in central and eastern Nepal but not in western Nepal. The relationship of extreme precipitation indices with topographic relief shows that extreme precipitation thresholds decrease with increasing elevation, but extreme precipitation days increase in higher elevation areas. Furthermore, stations above 1 km elevation exhibit a power-law relation in the rainfall magnitude-frequency framework. Stations at higher elevations generally have lower values of power-law exponents than low elevation areas. This suggests a fundamentally different behaviour of the rainfall distribution and an increased occurrence of extreme rainfall storms in the high elevation areas of Nepal.

1. Introduction

The water balance in the central Himalayan region depends primarily on the Indian Summer Monsoon (ISM) precipitation (Hannah et al., 2005; Bookhagen and Burbank, 2010). Solid precipitation impacts water budgets at high elevation and glacial mass balances, while the melting process and liquid precipitation significantly influence the downstream water balance (Hannah et al., 2005; Smith and Bookhagen, 2018; Norris et al., 2020). More than one-sixth of the world's population relies on rivers originating from the Himalaya as their principal source of water for livelihood and economic activities such as agriculture and hydropower (Nandargi and Dhar, 2011; Subash and Gangwar, 2014). During the ISM, high-intensity but low-frequency events occur (Wulf et al., 2010; Nandargi and Dhar, 2011). Extreme precipitation occurs during these events, which are the top 5–10% of all precipitation events (Bookhagen, 2010; Malik et al., 2012; Karki et al., 2017).

Recent discussions about the relationship between changing temperature and intensity-duration frequency of precipitation indicate the increase of extreme weather (both wet and dry) events and glacial retreat rate (Eriksson et al., 2009; Sheikh et al., 2014; Panday et al., 2015; Norris et al., 2020). However, there is not much clarity on the spatial patterns of extreme events (Malik et al., 2016; Stolbova et al., 2014, 2016). Hydrometeorological extreme events exhibit first-order control on the mass transport of water and sediment and a high rate of denudation in the steep terrains of the Himalayas (Thiede et al., 2004; Gabet et al., 2008; Bookhagen, 2010; Wulf et al., 2012). Therefore, the vulnerability of the Himalayan hydrological regime and socio-economic functions are often associated with extreme precipitation events, and some recent studies suggest the same for non-monsoon atmospheric rivers (Thapa et al., 2018). Nevertheless, a comprehensive overview of monsoon precipitation extremes in the Himalayan region is rare when compared to the rest of the world or South Asia (e.g., Barros et al., 2004; Haylock and Goodess, 2004; Anders et al., 2006; Malik et al., 2012; Malik et al., 2016; Karki et al., 2017; Ashcroft et al., 2019).

Extreme precipitation is associated with floods, landslides, and associated dam ruptures (Bookhagen, 2010; Wulf et al., 2010; Sheikh

Abbreviations: SMM, Summer Monsoon Month; WMM, Winter Monsoon Months.

* Corresponding author. Department of Forestry and Environmental Technology, South-Eastern Finland University of Applied Sciences, 50100, Mikkeli, Finland.
E-mail address: shakil.regmi@xamk.fi (S. Regmi).

https://doi.org/10.1016/j.wace.2022.100470
Received 3 September 2020; Received in revised form 28 February 2022; Accepted 2 June 2022
Available online 9 June 2022

et al., 2014). However, it is essential to note that extreme meteorological events trigger many disasters, but not every extreme event triggers a disaster. A recent example of dam rupture is the 2008 breaching of an embankment in the Koshi River due to sediment influx, which displaced about fifty-thousand people in southeastern Nepal and adjoining regions of India (Reddy et al., 2008). Likewise, extreme precipitation brought floods and landslides in Nepal's central and western mid-hills and southern plains on August 2014 and August 2017, respectively. In the former event, more than sixty-five thousand people got displaced, while in the latter, more than four-hundred thousand were displaced (IFRC, 2014; Bhandari et al., 2018).

Similarly, in June 2013, extreme precipitation triggered a flash flood in Saraswati and Mandakini Rivers in the northwest Himalayan region of India, damaging around three thousand houses (Prakash, 2018). The most recent event of inundation in July 2019 in central and eastern Nepal also displaced around ninety thousand people (Reliefweb, 2019). Recent findings suggest that these and similar disasters are often associated with increasing the intensity and frequency trend of extreme precipitation in central and western Nepal and the western Himalaya. For example, Karki et al. (2017) reported that extreme precipitation events are increasing in the southern plains, western mid-mountains, and central high mountains, along with an increase of dry days over east and central mid-mountains of Nepal from 1970 to 2012 using daily precipitation gauge data from 76 stations. Archer and Fowler (2004) also find an increase of precipitation events in parts of northeastern Pakistan (Upper Indus basin region), from the 1960s till the late 1990s, from 17 gauged stations. Large parts from western, central, and eastern India also show the increasing intensity and frequency trends of extreme rainfall events from 1951 to 2007 using daily gridded data with 0.5° horizontal resolution (Malik et al., 2016).

However, there is less consensus about precipitation trends (intensity and frequency) in the Himalayan mountains. There have been reports of no trends of monsoonal precipitation from 1948 to 1994 in Nepal, a decreasing trend from 1876 to 1982 in Shimla, in the western Himalaya, but also increasing (decreasing) trends of winter (summer) precipitation from 1964 to 1992 in the Beas catchment in the western Himalaya (cf. Archer and Fowler, 2004). Most studies of extreme precipitation in the Himalayan region focus on deriving linear decadal trends but less on its spatial pattern (cf. Malik et al., 2016). Chalise and Khanal (2002) and Baidya et al. (2008) find an increasing extreme precipitation trend in Nepal from 1971 to 1990 and 1961–2006, respectively. Although statistically insignificant, the trend of events in the Koshi River basin of eastern Nepal increased from 1975 to 2010 (Shrestha et al., 2017).

These findings are critical; however, the nature and pattern of extreme events are still underexplored in the Himalayan mountains. Nandargi and Dhar (2011) try to explain the nature of extreme events from Indian Himalayan states (1975–2000), Nepal (1921–1900), and Bhutan (1989–2005). However, their findings are generalised for the entire Himalayan range, and they report that one-day extreme rainfall occurs mainly between the Siwalik and the Himalayan peaks. Similarly, Panthi et al. (2015) find high precipitation days in the mountains than the Trans-Himalaya of central Nepal between 1981 and 2012 using 35 daily gauged data.

Barros et al. (2006) and Wulf et al. (2010) describe erosion and sediment-transport processes as a response to the catastrophic magnitude of flash floods and landslides associated with infrequent extreme precipitation events. The low (high) intensity and high (low) duration precipitation events assert different but consequential toll on various regions of the Himalaya (Dahal and Hasagawa, 2008). The landslide triggering and sediment runoff mechanisms are often analysed based on the impact of rainfall intensity-duration relation (Caine, 1980; Wulf et al., 2010; Alviolo et al., 2014). A different approach relies on estimating the magnitude-frequency relation and deriving a power-law exponent or regression coefficient of duration and magnitude (extent of intensity in mm/day). Magnitude-frequency relation has been used in the past to estimate the heavy tail of the rainfall distribution (i.e., rare and significant magnitude events) (Malamud and Turcotte, 2006; Rahmani et al., 2016). The power-law exponent describes the likelihood of heavy rainfall events: a smaller power-law exponent suggests a higher occurrence and magnitude of rare events (Wheeldon and Counsell, 2003; Clauset et al., 2009; Wulf et al., 2010; Tang et al., 2020). The power-law exponent of rainfall magnitude-frequency relations can describe the heavy tail of rainfall distributions and most often describes rainfall characteristics above the 99th percentile.

Extreme precipitation is also associated with ruptures of dams of glacial lakes, which pose a similar destructive threat. Regular satellite photos aid in predicting such ruptures and can be used in conjunction with rainfall prediction to identify hazardous events better. To better describe hydrometeorological extreme events and contribute to the current knowledge of ISM rainfall, we focus our study on the analysis of variability of precipitation patterns. Understanding a major local factor influencing ISM events has evolved gradually from elevation to topography and topographic relief (Barros and Lang, 2003; Barros, 2004; Anders et al., 2006; Bookhagen and Burbank, 2006, 2010). The variation in precipitation is high between the ridges and valleys along the southern face of the range. Furthermore, studies based on the Tropical Rainfall Monitoring Mission (TRMM) data shows a broad double-band of high precipitation in the southern slopes of central and western Himalaya with the first and second rise in topography (cf. Fig. 1) (Bookhagen and Burbank, 2006; Anders et al., 2006) but no studies analyse the consistency of the topography-precipitation relationship with in-situ gauge data.

The eastern Himalaya, east of Nepal, has a one-step rise of topography which shifts to a two-step rise towards the west (cf. Fig. 1a) (Bookhagen and Burbank, 2006). Nepal includes representative topography both of the eastern and western Himalaya. Although there are established studies on the relationship of topography with precipitation, the pattern of extreme precipitation events in relationship with the topography of the Himalayan range has not been addressed yet (Anders et al., 2006; Bookhagen and Burbank, 2006; Bookhagen, 2010). Specifically, Anders et al. (2006), Bookhagen and Burbank (2006), and Bookhagen (2010) document the relationship of precipitation bands with topographic steps, but the same is yet to prove in the case of extreme precipitation. Therefore, this study focuses on the relationship between topography and elevation with extreme precipitation in the central Himalaya during the ISM period.

We use 204 ground stations from Nepal (cf. Fig. 1c) to analyse the variability of extreme precipitation against the topography of the central Himalaya. The stations have 40 years of daily precipitation data from 1975 to 2014. The commonly used indices developed by the Expert Team on Climate Change Detection Monitoring and Indices (ETCCDMI) team were modified and used in this study (e.g., Croitoru et al., 2016). Indices of extreme events are percentile-based. The percentile threshold is objective and site-specific, allows comparison between different stations or regions, and is also associated with extreme precipitation events in the Himalayan region (Haylock and Goodess, 2004; Krishnamurthy et al., 2009; Bookhagen, 2010). The elevation of the stations ranges approximately from 70 m above sea level to 3 600 m. Since the stations above 2000 m are less common in previous studies (e.g., Archer and Fowler, 2004; Nandargi and Dhar, 2011; Wulf et al., 2012; Karki et al., 2017), their inclusion provides additional insights into the nature of precipitation and extreme precipitation events over the central Himalaya.

2. Geographic and climatic setting

The landmass of Nepal stretches ~885 km east-to-west and ~200 km south-to-north (Fig. 1a). Out of 147,181 km^2, about 83% of the country's land are hills and mountains (Dahal and Hasegawa, 2008). Based on the elevation ranging from ~60 m in the south to 8 848 m in the north, the geomorphology of Nepal consists of five elevational geologic units: Terai (<330 m), Siwalik (200–1 500 m), Lower Himalaya (500–3 000 m),

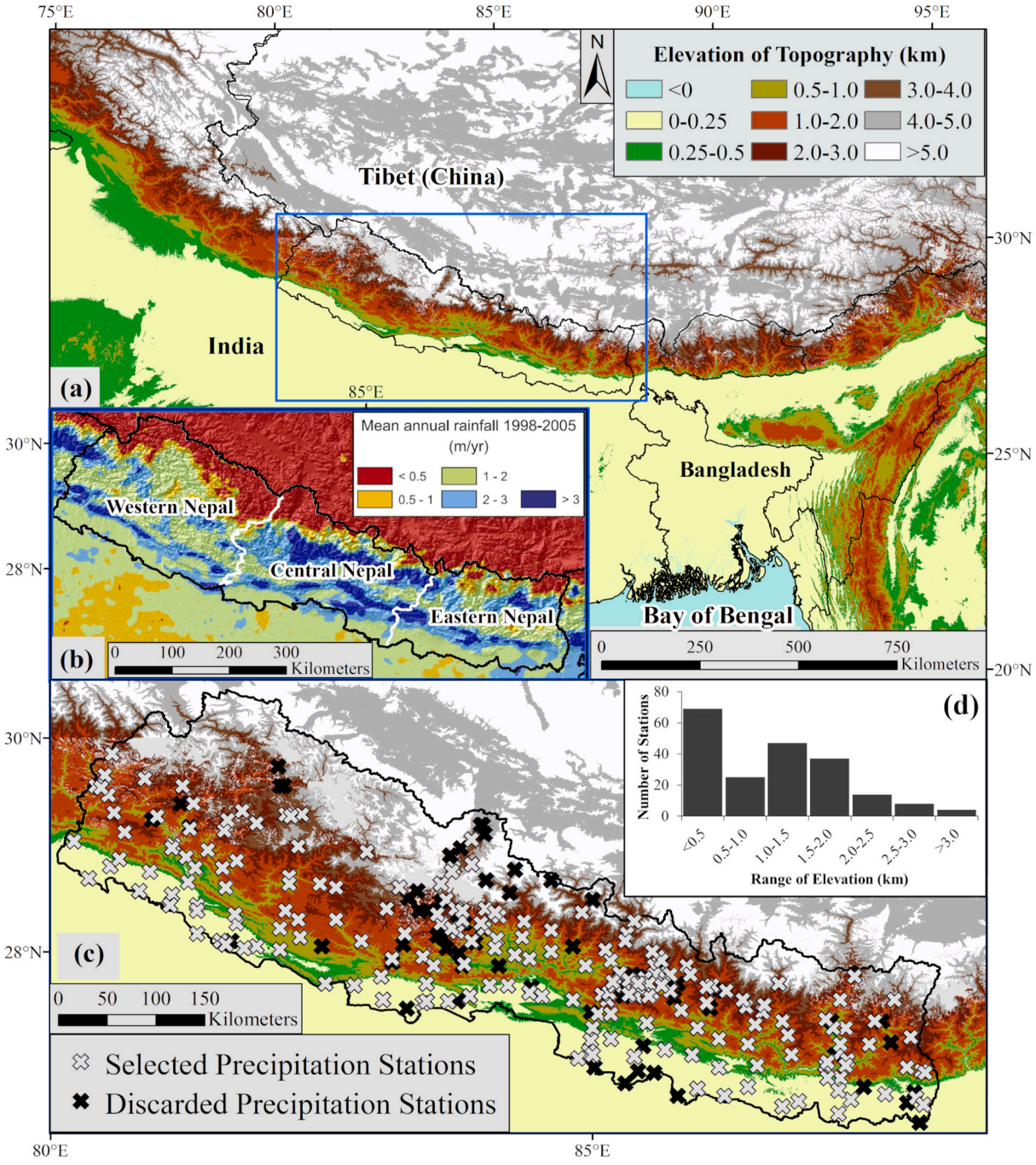

Fig. 1. (a) Digital topography of the Himalayan arc obtained from the Shuttle Radar Topography Mission (SRTM) with nominal 90m spatial resolution through the online portal of United States Geological Survey (USGS, 2012) and location of the study area in Nepal is outlined by the blue box. (b) Inset shows the average amount of annual rainfall calculated from the Tropical Rainfall Monitoring Mission with a spatial resolution of ~5 km × 5 km in Nepal between January 1998 to December 2005 (adapted from Bookhagen and Burbank, 2006), including the classification of the topographic swath profile of Nepal used in this study. (c) Selected 204 precipitation stations out of the total 274 ground stations from Nepal. (d) Frequency of the number of selected stations per elevation bins. (For interpretation of the references to colour in this figure legend, the reader is referred to the Web version of this article.)

Higher Himalaya (>2000 m) and Trans Himalaya (2 500–4 500 m) (Dahal and Hasegawa, 2008). The complexity of elevation zones with overlaps further demonstrates the precipitation variability related to the region's topography.

The east-to-west Himalayan range extends 2 400 km and functions as a natural barrier between the mid-latitudes and the tropics (cf. Fig. 1a). The Tibetan plateau sits north of the Himalayan range, and its elevated topography (average elevation ~4 km asl) faces rapid warming during the ISM period, compared to the surrounding oceans releasing latent heat leading to a low-pressure system which attracts the ISM onset, especially from the Bay of Bengal (Flohn, 1957; Webster, 1986). However, Liu and Dong (2013) find that the ISM and large-scale atmospheric circulation structures, even without the elevated Tibetan Plateau, show similar variability as currently observed. Their study highlights the importance of the Himalayan topography on the ISM.

At a synoptic scale, the ISM is part of the Inter-Tropical Convergence Zone which shifts the east-west oriented zone of high precipitation from the southern hemisphere during winter to the northern hemisphere

during summer (Bookhagen et al., 2005; Goswami, 2005). The low-level westerly jet from the Arabian Sea and a large-scale cyclonic vortex from the north of the Bay of Bengal to mainland India forms the ISM trough (Ding and Sikka, 2006). This circulation produces north to northwest directed moisture transport from the proximate Bay of Bengal.

During the ISM season, water vapour enters Nepal through the southern and eastern sides and exits through the northwest. The moisture originating from the Bay of Bengal travels north- and northwestwards and results in convection at the foothills of south-facing slopes and valleys of the Himalaya (for details on South Asian precipitation regime see: Webster, 1986; Barros and Lang, 2003; Barros et al., 2004; Bookhagen et al., 2005; Anders et al., 2006; Dimri, 2012). The ISM mainly occurs between May to October and accounts for ~80% of the annual precipitation in the Himalaya (Shrestha, 2000; Wulf et al., 2010; Panthi et al., 2015). On the other hand, the winter monsoon depends on the westerly disturbances, which are low-pressure systems in the mid-latitudes moving from the west to east (westerly) towards the subtropical region of Asia (Dimri et al., 2006; Cannon et al., 2017). The water vapour transported by these western disturbances converges in the Himalayan orography and undergoes intensification until the moisture content condenses and falls as precipitation (Barros, 2004).

As seen in Fig. 1, the topographic relationship with precipitation led to construe the critical role of relief, as pointed out by previous studies (Anders et al., 2006; Bookhagen and Burbank, 2010). Relief is related to erosion in the Himalayan orogeny system (Olen et al., 2015). Topographic relief increases with elevation until the main Himalayan divide (Fig. 2). In contrast, topographic relief in the Tibetan Plateau is low. Strong gradients in relief are known to increase precipitation peaks (Bookhagen and Burbank, 2006, 2010), but its relationship with extreme events is still unclear.

Furthermore, convective processes play an active role to form precipitation in the southern slopes of the Himalaya (Barros and Lang, 2003; Barros et al., 2004; Anders et al., 2006). In the Himalayan region, convection occurs mainly due to interaction with mountainous terrain. The thermal gradient between the troposphere and land dictates the diurnal (nocturnal) upslope (downslope) wind, which brings precipitation over the peaks (foothills) (Norris et al., 2020). These phenomena suggest that the precipitation is induced due to the atmospheric-orography interactions and is different at varying topographic gradients. Observation from Barros et al. (2000) found that elevation and the spatial arrangement of topographic gradients play an essential role in triggering precipitation. Barros et al. (2004) report a synoptic mode (~300 km) associated with the overall terrain envelope

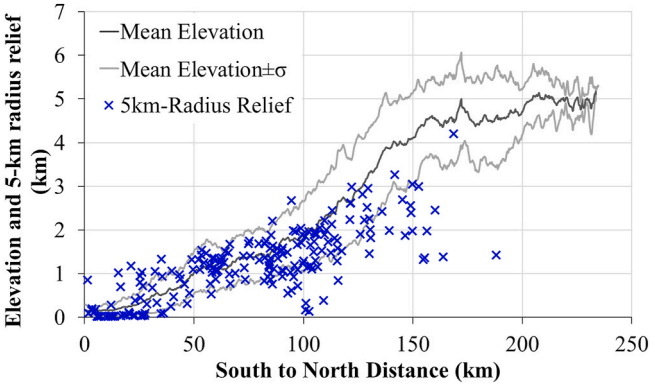

Fig. 2. The mean topographic profile and its standard deviation (σ) of Nepal and the height of 5-km radius relief from the selected ground stations (blue crosses) plotted against the south to north distance (cf. Fig. 1c for geographic location and swath extent). Each cross indicates the location of a gauge station. The linear correlation coefficient between elevation and relief is 0.72. (For interpretation of the references to colour in this figure legend, the reader is referred to the Web version of this article.)

and the major river valleys, and a quasi-periodic succession of ridges and valleys that constitute the Himalayan range about 5 km–150 km from the mountain front as two distinct types of orographic controls. These occur at different spatial scales after conducting a comparative analysis between the collocated variability of topography and the overlying cloud cover.

To date, researchers have identified the arrival of onset, location, and formation of convection as significant processes responsible for precipitation in the Himalaya (e.g., Barros et al., 2000; Barros and Lang 2003; Anders et al., 2006; Wulf et al., 2010; Bookhagen, 2010; Stolbova et al., 2016). On the other hand, extreme precipitation occurs due to various interrelated reasons such as synoptic-scale rainstorms, sudden cloudbursts, high winds, atmospheric rivers and snowstorms (Barros et al., 2004; Nandargi and Dhar, 2011; Thapa et al., 2018). The extreme events occur during the active monsoon period (Malik et al., 2012) but shows no coupling with the annual or seasonal rainfall distribution in the high mountainous regions (Bookhagen, 2010). These events also occur during the synoptic-scale rainstorms, different from local convective events (Barros et al., 2004).

3. Data and method

3.1. Data

The precipitation data from 274 stations were collected from the Department of Hydrology and Meteorology of Nepal (DHM). The data consist of daily (24 h) observed precipitation (starting from 9 a.m. the previous day) in millimetres (mm). The DHM uses a US-standard 8-inch (20.32 cm) diameter manual precipitation gauge and has a well-accepted less than 15%-gauge error uncertainty (cf. Dulal et al., 2006; Talchabhadel et al., 2016). In the case of snowfall, the snow water equivalent is measured by melting the collected snow and then converted to standard rainfall measurement. In addition to evaporation, wetting and splashing error, the wind error is known to significantly increase the uncertainty of snow record while the uncertainty for rainfall is not high (cf. Talchabhadel et al., 2016). However, our study mainly focuses on the summer monsoon period, where the impact of snowfall is minimal.

In order to include all the stations with equal data length, stations with data from 1975 to 2014 are included, while the data uncertainty factor was not considered in station finalisation due to its uniform nature and an accepted standard value for uncertainty (cf. Dulal et al., 2006). Any stations with years of data gaps of more than 20% or leading to less than 40 years of data were omitted to obtain the final list of the stations (cf. Bohlinger and Sorteberg, 2018). This selection process led to the removal of 70 stations, shown in Fig. 1c. Outliers in the data were not removed because (1) the DHM controls them by removing outliers and negative values and (2) not to miss the extreme events (cf. Bohlinger and Sorteberg, 2018). Days with data gaps (2% out of the total data days) were left blank during the calculation. The small amount of missing data did not significantly affect the calculated extreme-event statistics. The Digital Elevation Model (DEM) of Nepal was obtained from the Shuttle Radar Topography Mission (SRTM), nominal 90 m spatial resolution through the online portal of the United States Geological Survey (USGS, 2012).

3.2. Methods

The topography of Nepal varies from west to east. To address this, we analyse south to north topographic swath profiles separated into western, central and eastern Nepal (cf. Fig. 1b). The swath profiles were divided approximately by an equal distance of longitudes, taking into account the boundary of state districts. The elevation of topography and relief was calculated from the SRTM DEM of Nepal. Topographic relief is the difference between the maximum and minimum elevation within a given radius; for example, in this study, we rely on a 5-km radius area

around the location of each station. Station statistics were calculated based on the indices presented in Table 1.

The indices adapted from the ETCCDMI (Croitoru et al., 2016) consist of the 95th percentile threshold, the extreme precipitation threshold used in this study. We used three different timeseries to analyse the collected data and calculate the indices mentioned in Table 1: the annual and seasonal timescales. The seasonal timescales are Summer Monsoon Months (SMM, from May to October) and Winter Monsoon Months (WMM, from November to April). The SMM dominates extreme precipitation events (Malik et al., 2012). While large rainfall magnitudes do not occur during the WMM, we have included these statistics to provide a holistic analysis. The calculated values were represented graphically or spatially. These represented values were categorised based on the stations and the study's needs, such as the elevation or relief. We also evaluate the station statistics within elevation bins of 500 m from ≤500 m to ≥3 000 m for comparative analysis. The pattern of extreme precipitation was also examined visually by calculating the difference of extreme precipitation from mean precipitation events. To allow for a spatial comparison, we divide the 95th percentile precipitation threshold by the 50th percentile threshold to observe the distribution of precipitation intensity. We refer to this value as the median normalised extreme precipitation value.

In a second step, we use the magnitude-frequency relation of the rainfall time series to estimate extreme events. The magnitude is the size of daily mean rainfall intensity, i.e., amount of precipitation in mm per day of each rainfall event. Each event consists of the sum of at least three or more continuous days of precipitation (at least >1 mm with the possible inclusion of a one-day gap with no precipitation). We perform magnitude-frequency analyses in different elevation bins and estimate the power-law exponent and power-law fit using a maximum likelihood method (Clauset et al., 2009). Clauset et al. (2009) argue that Pareto's logarithmic scale chart following approximately a straight line and estimating power-law exponent by performing least-square linear regression generates significant errors under relatively common conditions (Arnold, 2015). Thus, they propose estimating a minimum value (x_{min}) above which a power law holds. The regression slope is denoted by α and determined using maximum likelihood estimation. The goodness-of-fit value is estimated by applying one thousand iterations between the data and power-law using the Kolmogorov-Smirnov test to find the p-value (cf. Clauset et al., 2009). The scaling parameter or power-law exponent (α) was calculated using Equation (1).

$$\alpha = 1 + n\left[\sum_{i=1}^{n} ln\frac{x_i}{x_{min}}\right]^{-1} \quad \text{Equation 1}$$

In Equation (1), x_i, $i = 1, \ldots, n$, are the observed values of x where $x_i \geq x_{min}$. Here, x is the available set of data and x_{min} is the lower bound of power-law behaviour in the data. The selection of x_{min} is critical because a too low value will bias the slope regression, and a too high value will exclude genuine data points. Thus, the value which minimises the Kolmogorov-Smirnov statistic is the best estimate of the x_{min} calculated using Equation (2) (Shatnawi and Althebyan, 2013). A smaller exponent indicates negatively skewed data and suggests a higher magnitude of rare events (Wheeldon and Counsell, 2003).

$$D = \max|S(x) - P(x)| \quad \text{Equation 2}$$

Where D denotes the Kolmogorov-Smirnov statistic. $S(x)$ is the cumulative distribution function (CDF) of the values with at least x_{min} from the observed data, and $P(x)$ is the CDF for the best-fitted model when $x \geq x_{min}$. After estimating α and x_{min}, the hypothesis of power-law fit was tested with the goodness-of-fit to calculate the p-value (Clauset et al., 2009). If the p-value is greater than 0.1, the data are described by a power-law behaviour. Thus, x_{min} is a vital threshold for identifying the skewness point, suggesting higher precipitation intensity occurrences. The uncertainties of x_{min} and α were also estimated to ensure the reliability of the power-law behaviour, which were calculated by using a nonparametric bootstrap method as described by Clauset et al. (2009).

Table 1
This study used a list of indices adapted from the Expert Team on Climate Change Detection Monitoring and Indices (ETCCDMI) (Croitoru et al., 2016).

Index	Name	Description
R0.1	Precipitation days	Number of days with >0.1 mm precipitation
PRCPTOT	Precipitation amount	Total amount of daily cumulated precipitation
R95	Extreme precipitation threshold	95th percentile threshold of daily precipitation
R95d	Extreme precipitation days	Number of days above R95
R95p	Extreme precipitation amount	Total accumulated precipitation amount > R95

4. Results

4.1. Daily seasonal extreme precipitation and its relationship with the topography

The SMM receives more than 90% of the annual PRCPTOT and ~85% of the annual R0.1. The high proportion suggests a similar pattern of indices between annual and SMM events. Our result and discussion session comprise mainly of SMM except for the part concerning Fig. 6. We find that the SMM R95p comprises approximately 25% of the annual PRCPTOT. Contrary to that, SMM R95d is 5% of the annual R0.1, aligning with the definition of the 95th percentile. Observations from Fig. 3 and Fig. 4 show that the pattern of mean SMM PRCPTOT (precipitation amount) and mean SMM R95p (extreme precipitation amount) differ in the plains compared to high elevation regions. Specifically, the percentage ratio of R95p in the lowest elevation region (<0.5 km) is higher than the same ratio of PRCPTOT compared to other elevation regions. Except for activity in the plains, the pattern of R95p in central Nepal resembles that of PRCPTOT, i.e., peaks in 0.5–1 km and 1.5–2.5 km. Similarly, R95p peaks and increases at < 0.5 km and 1–1.5 km and decreases at a higher elevation than the mean PRCPTOT in eastern Nepal.

Interestingly, SMM mean PRCPTOT and R95p in eastern and central Nepal rise with an orographic peak, but mean R95p is higher also in the plains (cf. Fig. 3). Importantly, there is a similarity between eastern Nepal's PRCPTOT and R95p in the plains and the first rise of topography. In addition, the higher values of R95p in the plains of Nepal suggest a higher impact of monsoonal depression in this region. Likewise, the total and extreme indices in the west are lower at higher elevations, with a maximum on the first rise of topography but not on the second. These observations suggest a prominent role of topography near the onset but not in the outlying areas from the onset.

The R0.1 is higher in higher elevations than at lower elevation areas (cf. Fig. 3g–i). However, annual mean values of both PRCPTOT and R0.1 drop around 1.1 m and 50 days, respectively, above 2.5 km elevation across Nepal. The lower values of all four indices from Fig. 3 in western and central swaths represent the arid leeward side of the Himalayan range. The peaks of PRCPTOT suggest a relationship with topography, but when averaged, there is not much difference in higher and lower elevation stations. In contrast, the R0.1 has a positive difference of around 30 days between lower (<1 km) and higher elevation stations, supporting its relationship with elevation rather than topography. As seen in Fig. 3g-l, the occurrence and pattern of R95d are similar to that of R0.1. The R95d is around three-fold higher than the lower elevation of central and eastern Nepal, and the same is two-fold in western Nepal.

Fig. 5 shows that the R95 decreases with elevation during the SMM. Our findings show that the first orographic rise receives high-intensity precipitation in fewer days, while the second orographic rise receives comparatively lower-intensity precipitation in more days. However,

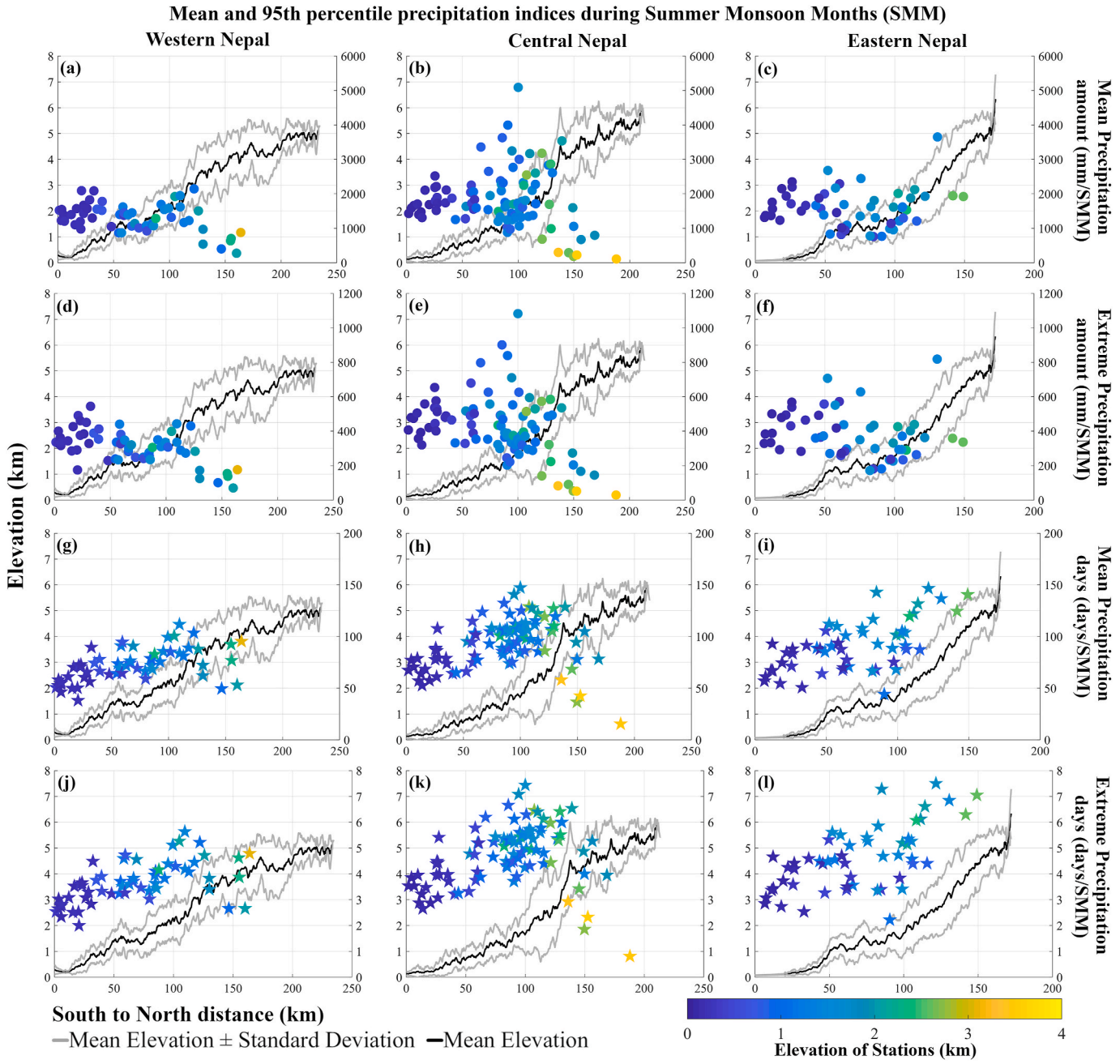

Fig. 3. South-to-north topographic profile of western, central, and eastern Nepal showing the 95th percentile values during [1975–2014] Summer Monsoon Months (SMM, i.e., May–October). The circles represent mean precipitation amount (PRCPTOT) and mean extreme precipitation (R95p) in the first and second row, respectively, while the stars represent precipitation days (R0.1) and extreme precipitation days (R95d) in the third and fourth row, respectively. The colour variation of each station represents its elevation. The grey and black lines show ± standard deviation of elevation and mean elevation of the topographic orientation of the study swaths, respectively. (For interpretation of the references to colour in this figure legend, the reader is referred to the Web version of this article.)

there is not much difference in the precipitation received at the first and second rise of topography. In contrast, the R95 during the WMM shows uniformity until 3 km elevation. The intensity of extreme precipitation during the winter is, thus, similar in the plains and the hills (cf. Fig. 5).

Western Nepal is the most affected region by the winter westerly, as it generally enters Nepal from the western direction. As seen in Fig. 6 (second row), the mean WMM R95p (extreme precipitation amount) during the winter in western Nepal is higher, except in the trans-Himalaya zone, which are the arid interiors of the Himalayan range. Interestingly, central Nepal shows a similar pattern to that of the SMM. On the other hand, the highest point in eastern Nepal shows larger values. Our observations suggest that winter westerly storm systems propagate into the study area and nearly equally impact mid and high elevations. The higher altitude of these storms allows deeper penetration into the orogen – in contrast to the summer season, where convective storms relate to the topography.

Revisiting the SMM precipitation events compared to the topographic 5-km radius relief as seen in Fig. 7, our observations suggest that the precipitation indices show a similar pattern compared with relief or topography. However, some high-relief stations show higher numbers of extreme precipitation days, while the same relationship for extreme precipitation amount exists in central Nepal at mean elevations of ~2 km (cf. Fig. 7). As construed, the R0.1 peaks in higher elevation in all three regions of Nepal with at least a three-fold increase compared to the

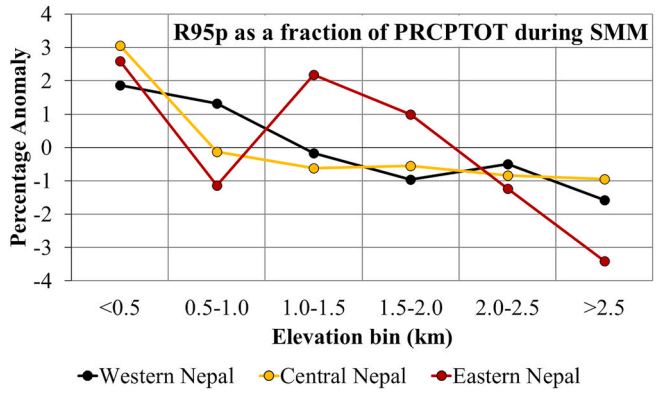

Fig. 4. Percentage anomaly of the mean value of R95p per elevation bin as a fraction of mean value of PRCPTOT per elevation bin for western, central and eastern Nepal during Summer Monsoon Months (SMM, i.e., May–October). Positive anomaly values refer to a higher percentage of R95p compared to that of PRCPTOT. This shows that the plains have a more R95p percentage ratio than higher elevation, where the difference pattern is almost similar.

lower elevation. The R95 shows contrasting characters compared to R95d. Although there is a similarity in R95's relationship with relief and elevation, there are noticeable peaks of its high values in high relief regions of western and central Nepal. Though, eastern Nepal shows a comparatively higher similarity of relief and topography. The R95p shows an identical pattern to that against topography (cf. Fig. 3), which indicates the role of relief in the pattern of precipitation.

4.2. Daily spatial distribution of extreme precipitation events

The relationship of PRCPTOT with topography and R0.1 with elevation is also seen in Fig. 8. In addition, higher spatial distribution is concentrated in Nepal's central and eastern parts. The PRCPTOT increases by around 0.4 m while R0.1 increases by approximately 20 days from west to east. Specifically, higher R95d in the central-north and northeastern parts indicate a high risk of erosion in the arid high Himalayan regions. Furthermore, the high and almost uniform occurrence of R95 in the southern plains of Nepal compared to hills and mountains show a different pattern than R95p and R95d.

The higher value of indices in the south and east of Nepal indicate the impact of monsoonal onset, which enters Nepal from southern and eastern points and dominates the proportion of annual precipitation events. The departure of R95 from its median, i.e., 50th percentile precipitation threshold, shows the width of rainfall distribution and its spatial pattern (cf. Fig. 9). The ratio of median normalised extreme precipitation threshold, when higher, suggests the concentration of extreme events. Fig. 9 shows that the lower elevation and relief regions receive more extreme precipitation. However, eastern Nepal's mid-elevation and relief regions of 1–2 km also show higher proportions. Interestingly, the variation of median normalised 95th percentile precipitation threshold decreases by a factor of two from the mountain front to the orogen interior.

Our findings show an almost similar amount of extreme precipitation in fewer extreme precipitation days in low elevation regions. In comparison, similar extreme precipitation occurs in a more significant number of extreme precipitation days in high elevation regions, both being associated with the topographic gradients. However, in Fig. 8d, we observe that some high extreme precipitation days occur mainly in central and northeastern regions.

4.3. Precipitation magnitude-frequency relation for three or more days

Table 2 shows that most stations below 1 km elevation do not exhibit a power-law behaviour as indicated by a low p-value (<0.1).

Contrary to that, the magnitude-frequency relation of the stations above 1 km exhibit a power-law behaviour. We observe that rare and high magnitudes exhibit different scaling behaviours between lower and higher elevations (cf. Fig. 10). We document that power-law exponents change with elevation (cf. Table 2) and suggest that higher elevation

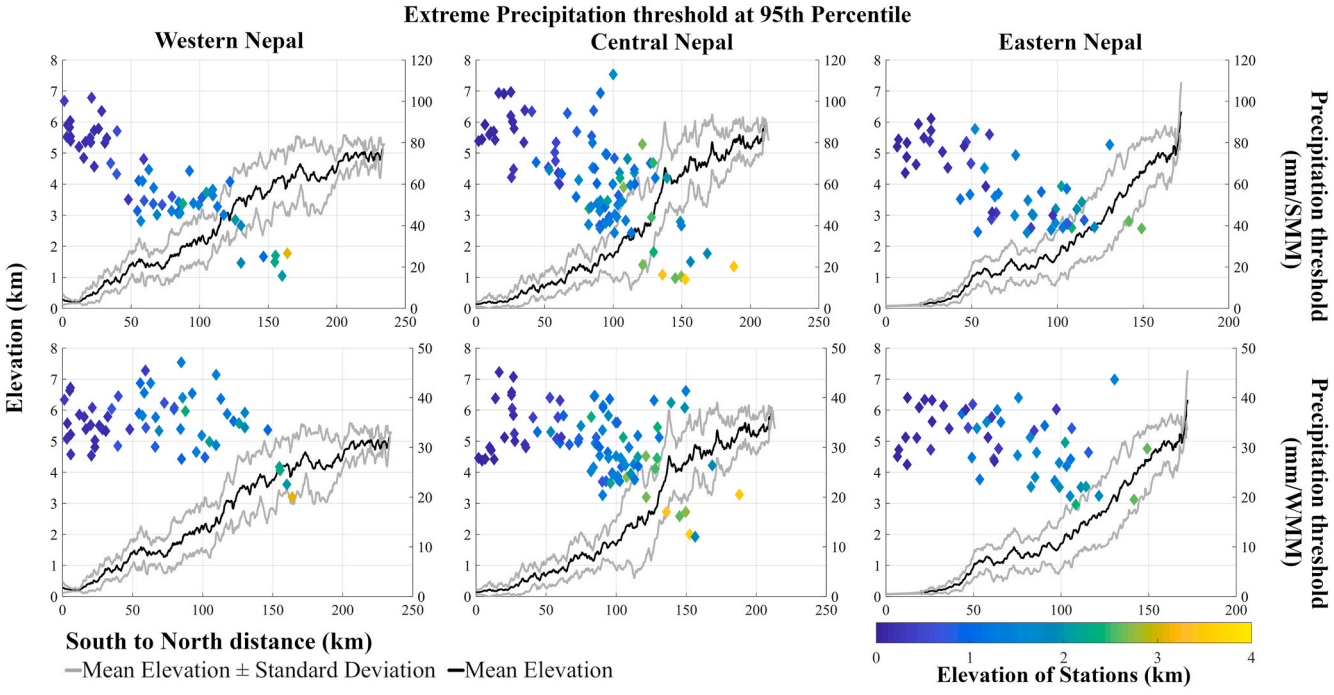

Fig. 5. South-to-north topographic profiles of western, central, and eastern Nepal showing the 95th percentile threshold during Summer Monsoon Months (SMM, i.e., May–October) and Winter Monsoon Months (WMM, i.e., November–April). The colour variation of each station represents its elevation. Note the different precipitation threshold scales between SMM and WMM. (For interpretation of the references to colour in this figure legend, the reader is referred to the Web version of this article.)

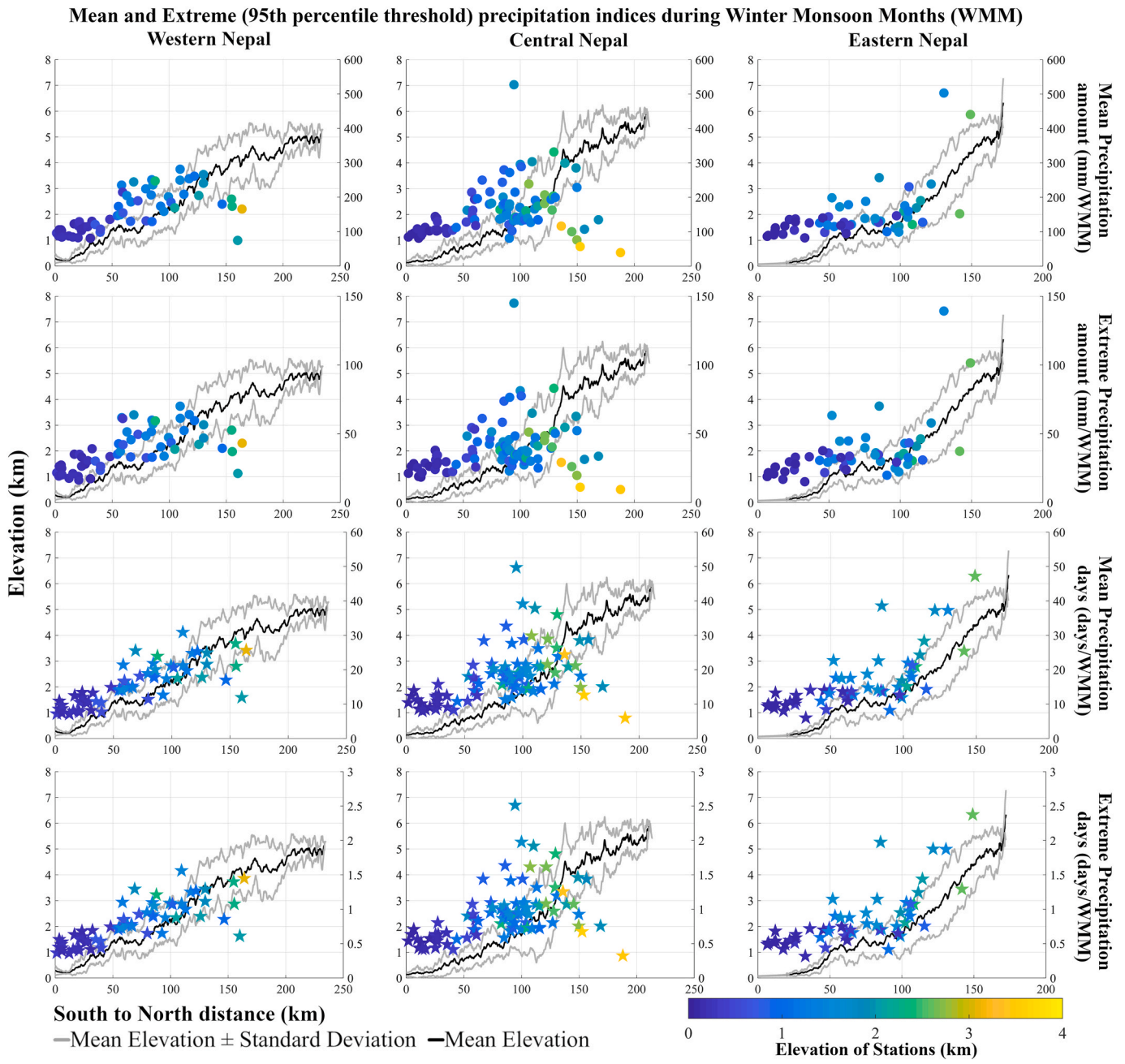

Fig. 6. South-to-north topographic profile of western, central, and eastern Nepal showing the 95th percentile values during Winter Monsoon Months (WMM, i.e., November–April). The circles represent precipitation amount, while the stars represent precipitation days. The colour variation of each station represents its elevation. (For interpretation of the references to colour in this figure legend, the reader is referred to the Web version of this article.)

terrain have higher numbers of high magnitude-intensity events. These could be non-extreme events based on our percentile threshold analysis but shows the probability to cause environmental distress in the higher elevation regions. We note that the precipitation threshold at which we observe a power-law behaviour (x_{min}) also decreases. The higher elevations thus show more occurrence of the very extreme events (>99th percentile cf. Fig. 11), which are also the rare and top events within the 95th percentile values.

Note the concentration of high extreme precipitation days in the higher Himalaya region in Fig. 11b than that of the 95th percentile threshold (cf. Fig. 8). Hence, higher-elevation regions experience more of Nepal's rarest and highest precipitation events. This finding has been partly suggested by analysing fewer rainfall stations in the western Himalaya (Wulf et al., 2010).

5. Discussion

Previous studies discern various patterns of precipitation in the Himalayan range (Burbank et al., 2003; Barros and Lang, 2003; Archer and Fowler, 2004; Barros et al., 2004; Anders et al., 2006; Bookhagen and Burbank, 2006; Bookhagen, 2010; Malik et al., 2012; Panthi et al., 2015; Norris et al., 2020). These studies use ground station data or the satellite data from the Tropical Rainfall Monitoring Mission (TRMM) with ~5 km or ~30 km (product 3B42) horizontal resolution or the interpolated APHRODITE (55 km horizontal resolution) data. The presence of ridges and steep topography in the Himalaya with lower width than data or model grid sizes may result in under or over-representation of the precipitation amounts (Barros et al., 2006; Anders et al., 2006; Andermann et al., 2011; Yatagai et al., 2012; Cannon et al., 2017). On the other

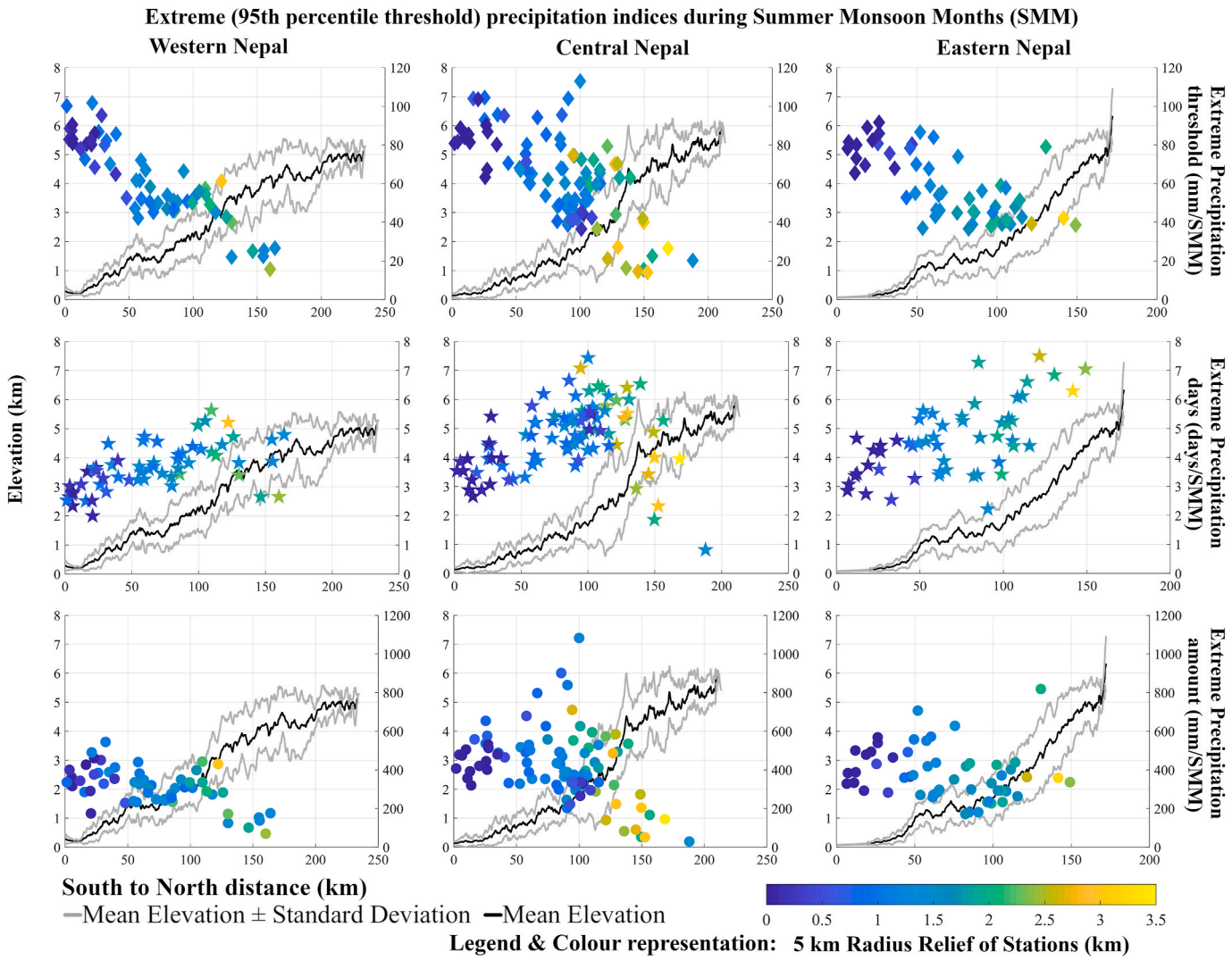

Fig. 7. Relation between 5-km radius relief calculated for each station location and its relationship with the values of extreme precipitation threshold, days and amount during Summer Monsoon Months (May–October). When compared to relief, the precipitation indices show a similar pattern to elevation or topography, but we observe high relief stations with high precipitation in central and eastern Nepal. The colour variation of each station represents its 5-km radius relief height. (For interpretation of the references to colour in this figure legend, the reader is referred to the Web version of this article.)

hand, the studies of extreme precipitation in the Himalaya using ground stations focus mainly on smaller regions or linear trends, while only a few studies focus on its variability (Singh & Kumar, 1997; Barros et al., 2006; Chalise and Khanal, 2002; Karki et al., 2017). We attempt to decipher the extreme events' topographical variability with a percentile threshold, a magnitude-frequency analysis, and their respective power-law regression.

5.1. Daily extreme precipitation

The topographic setting of Nepal represents the Himalaya range. The western and eastern Himalaya have a one-step rise, while the central Himalaya has a two-step rise (Bookhagen, 2010). Similarly, there is a two-step in central, moderate two-step in western, and a one-step rise in eastern Nepal. Importantly, our results of extreme precipitation align with these previous studies. The extreme precipitation in eastern Nepal shows a one-band increment while central Nepal shows a double-band (cf. Figs. 3 and 8). On the contrary, western Nepal exhibits a weaker two-step morphology that does not result in a double-band of extreme precipitation (cf. topographic profiles in Fig. 3). However, the similarity between total precipitation and extreme precipitation amounts differs in the low-elevation plains. The 95th percentile precipitation (R95p) ratio is more in the plains of Nepal than the mean precipitation amount (PRCPTOT).

Likewise, the extreme precipitation threshold is high in the plains in all three parts of Nepal and decreases with elevation. In addition, the Himalaya mountain front at ~1 km elevation receives more than a two-fold proportion of extreme precipitation threshold than the orogen interior. The plains have lower topographical disturbance and higher temperatures than the hills and mountains (Shrestha and Aryal, 2011) and exhibit strong local convective events. Also, the extreme precipitation threshold is higher in the low elevation because the warmer air column or water vapour can store a more considerable amount of precipitation.

Contrary to that, we find the number of days of extreme precipitation increases with increasing elevation in Nepal, which has a similar spread of pattern similar to the mean precipitation days. Hence, the impact on the higher elevation region is significant in the central Himalaya. As discussed above, the plains of Nepal receive higher extreme precipitation amounts in fewer days (cf. Fig. 3). Interestingly, these events have high 95th percentile thresholds (cf. Fig. 5). Thus, the risk of imminent inundation is high at the plains. For example, on 11–12 July 2019, the southern districts of Nepal (<300 m), Simara and Janakpur, received 311.9 mm and 245 mm of rainfall within 24-h, respectively. These

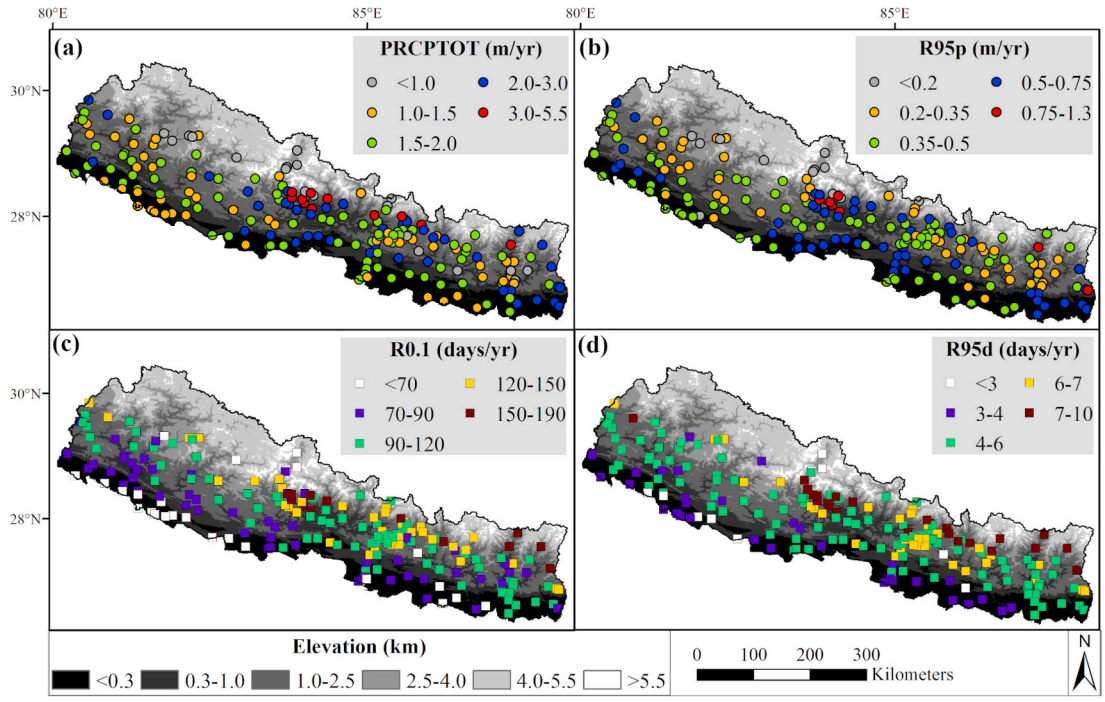

Fig. 8. Spatial distribution of annual mean and extreme precipitation events in Nepal. (a) Mean precipitation amount. (b) Extreme precipitation amount (above 95th percentile threshold event accumulation). (c) Number of mean precipitation days. (d) Number of extreme precipitation days. The circles indicate precipitation amount, and squares represent the number of precipitation days.

localised extreme events flooded the region and resulted in twenty-nine casualties, while more than two thousand households were temporarily displaced (United Nations, 2019). The entire episode in south-central and eastern Nepal in July 2019 resulted in more than one hundred casualties, while half of the households lost more than 75% of their food stock (Government of Nepal, 2019).

Next, we test the relationship between precipitation and elevation and between precipitation and topography, including topographic relief in Nepal. Topographic relief is ultimately shaped by the river incision and the geologic evolution of the Himalaya (Bookhagen and Burbank, 2006). We use a 5-km radius from the station's location to calculate the relief height. The relationship of maximum extreme precipitation amount with topography in three swaths of Nepal may also suggest (cf. Fig. 3) a relationship with topographic relief (cf. Fig. 7). Previous studies using remotely sensed data had shown the relief effect with a sudden rise of precipitation with an abrupt increase of relief (Bookhagen and Burbank, 2006; Bookhagen, 2010).

In contrast, we do not find this relationship regarding extreme precipitation amount. It is important to note that not all reliefs at the stations' locations are prominent enough to trigger extreme precipitation events. However, few stations with high relief experience high extreme precipitation days and receive high extreme precipitation, specifically in central and eastern Nepal. Interestingly, the lower activity of extreme precipitation concerning western Nepal's topographical characters can be attributed to its greater distance from the onset of a monsoonal depression.

Moreover, the average difference between the 95th percentile precipitation amount in the first orographic rise (at ~1 km mean elevation) and the second orographic rise (at ~2 km mean elevation) is only 12 mm during the summer monsoon months. However, the first orographic rise receives high-threshold precipitation in fewer days, while the second orographic rise receives comparatively low-threshold precipitation in more days (cf. Figs. 3 and 4). Thus, while extreme precipitation is similar, the threshold and duration of rainfall differ.

5.2. *Precipitation magnitude-frequency relation*

In order to better investigate the behaviour of extreme rainfall events, we have analysed the precipitation magnitude and frequency relation. The vulnerability of high elevation is further supported by the lower values of power-law scaling exponent (α) in high elevation regions of Nepal. The findings suggest that the High-Himalaya regions experience rare high magnitude-intensity events, which are not recognised by the pattern of extreme precipitation events defined by the 90th percentile. We have discussed our finding of a larger number of extreme precipitation days in high elevation regions, and we complement this analysis by looking at the highest percentiles (>99th percentile). This analysis indicates that higher elevation receives a larger number of very rare, very high rainfall events as indicated by a lower slope in the power-law relation (cf. Figs. 10 and 11). Occurrences of such rare but high magnitude precipitation events at the mountain front and in the semi-arid orogen interior will impact the river and sediment runoff and lead to enhanced erosions and flash floods.

Specifically, the hills receive extreme precipitation at a comparatively low 95th percentile threshold but almost similar 95th percentile precipitation over an extended period. An increase in extreme precipitation events can lead to enhanced erosion and hillslope instability in the Nepalese Himalaya (Burbank et al., 2003; Hannah et al., 2005). In addition, the steep gradients have a steady erosion rate directly related to the precipitation rate (Gabet et al., 2008). Bookhagen et al. (2005) report high denudation rates in low to medium elevation parts of the orogen during abnormally wet years or strong monsoon years. Some of these events are instrumental in shaping the landscape in the orogen interior by triggering debris flow (Bookhagen et al., 2005).

Plains and hills have different topographic characters, yet the impact of the hillslope instabilities, especially landslides and severe flooding, is imminent in both regions (Chalise and Khanal, 2002; Burbank et al., 2003; Hannah et al., 2005; Dahal and Hasagawa, 2008; Nepal, 2016). These are common environmental problems of Nepal and will cause stress in the socio-economic structure of the region. For example, the primary source of livelihood of most communities in Nepal is farming

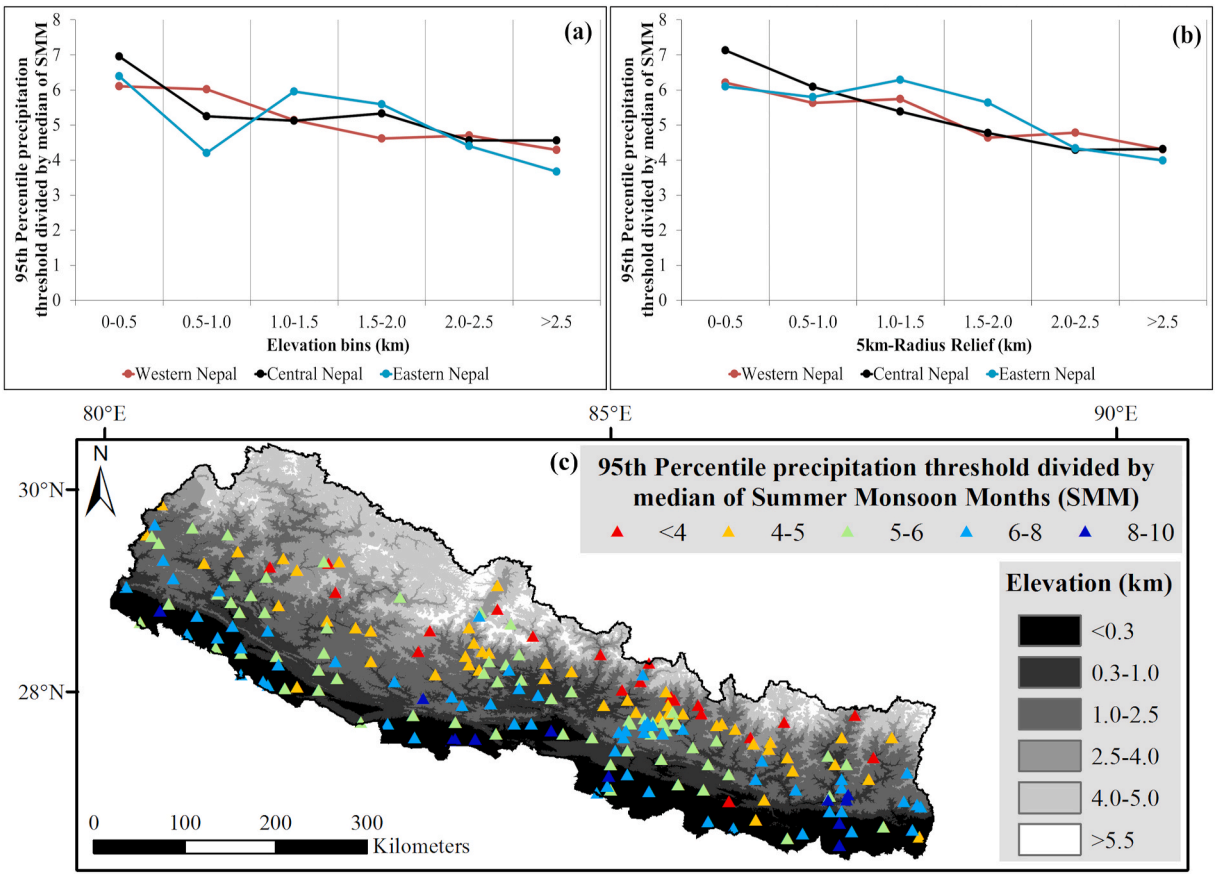

Fig. 9. Spatial distribution of extreme precipitation in Nepal elaborated by showing the 95th percentile extreme precipitation threshold divided by the median (50th percentile precipitation threshold) during the Summer Monsoon Months (a) against elevation bins; (b) against 5 km-radius relief; and (c) over the digital elevation model of Nepal. At the mountain front at the first topographic rise, the 95th percentile is more than 6–8 times higher than the median precipitation. In the orogen interior, this relationship is halved.

Table 2
Power-law regression values for magnitude-frequency precipitation of the stations from each elevation bin using a maximum likelihood estimator (cf. Clauset et al., 2009). Bold p-values indicate a statistically significant power-law behaviour.

Elevation Bins	Number of Stations in bin	Scaling exponent (α)	α error	x_{min}	x_{min} error	p-value
<0.5 km	69	5.25	0.58	58.33	11.26	0.00
0.5–1.0 km	25	4.83	0.25	30.93	3.30	0.09
1.0–1.5 km	47	5.19	0.26	36.72	4.30	**0.80**
1.5–2.0 km	37	5.48	0.32	34.32	3.20	**0.42**
2.0–2.5 km	14	6.21	0.47	28.75	2.09	**0.76**
2.5–3.0 km	8	4.55	0.49	19.21	3.23	**0.11**
>3.0 km	4	4.20	0.50	10.50	2.11	**0.38**

(Chalise and Khanal, 2002). Thus, the land deterioration caused by floods and landslides will significantly negatively impact the region's farming.

6. Conclusion

This study used 40 years of daily precipitation data from 204 ground stations in Nepal. The stations' elevation ranged from 72 m to 3 609 m and were analysed by adapting the indices set by the Expert Team on Climate Change Detection Monitoring and Indices (ETCCDMI) based on a 95th percentile extreme precipitation threshold. We also calculated the magnitude-frequency relationship to constraint low frequency, high magnitude events. The key conclusions are elaborated below.

First and most importantly, we observe discrete peaks of extreme precipitation values in relationship with the topographic parameters in the Himalaya. The Himalayan topography has a moderate and prominent two-step rise in western and central Nepal, respectively and a one-step rise in eastern Nepal. The first rise occurs on the frontal regions of the Himalaya with a mean elevation of ~1 km, while the second inner rise occurs at around ~2 km. Simultaneously, central and eastern Nepal show a double and single-band of peak values of extreme precipitation, respectively, but western Nepal shows none due to its distance from the ISM onset, which is our significant finding. On average, ~24% precipitation falls above the 95th percentile out of the mean annual precipitation for all stations.

Secondly, the 95th percentile extreme precipitation threshold value decreases with elevation. However, the number of extreme precipitation days increases with elevation, and these relations are different during the winter and summer seasons. Specifically, all analysed indices show greater concentration in higher elevation zones of Nepal during the winter seasons. One major significance is the non-relationship of extreme precipitation with elevation but a negative linear relationship of extreme precipitation threshold with elevation. In general, the extreme precipitation peaks coincide with topographic peaks but decreases from south to north. Since extreme precipitation decreases in the higher elevation zones, the threshold also decreases. To incorporate the entire topographical feature, we did not find any significant role of topographical aspect to influence the precipitation pattern except the high ratio of extreme precipitation and threshold in the plains in contrast to the total precipitation.

Third, and to better constrain rainfall distribution in Nepal, we analysed the magnitude-frequency relation of precipitation time series

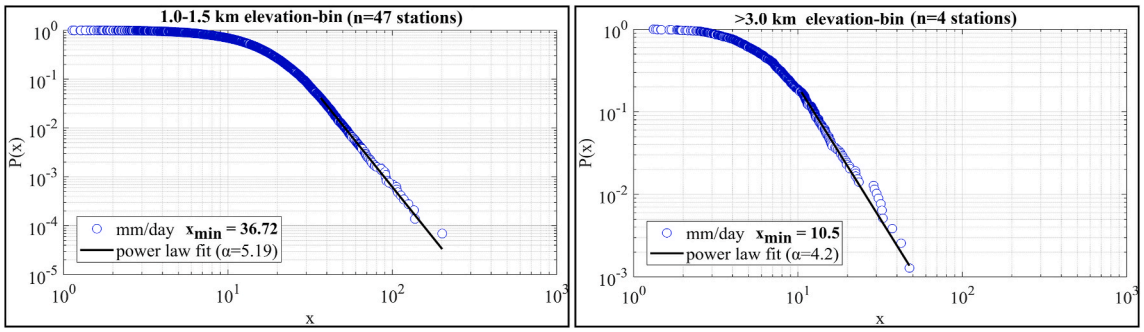

Fig. 10. Magnitude-frequency relation using daily precipitation measurements (at least three or more consecutive wet days >1 mm/day) and the power-law regression following Clauset et al. (2009) for two elevation bins of all station data with elevations of 1–1.5 km (n = 47 stations) and with an elevation of >3 km (n = 4 stations). Respective scaling exponent and x_{min} are given for both regressions.

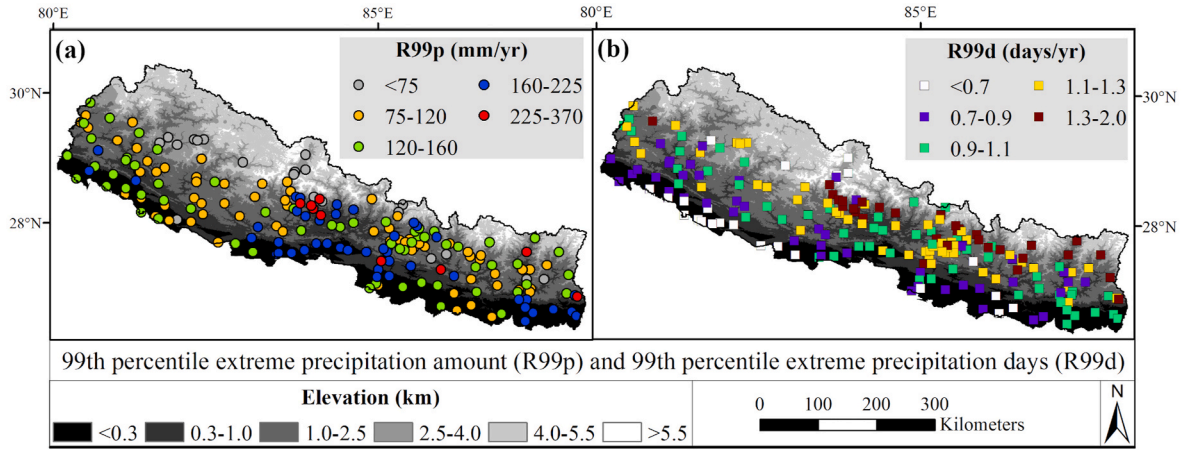

Fig. 11. Spatial distribution of 99th percentile extreme precipitation events in Nepal. (a) Extreme precipitation amount. (b) Number of extreme precipitation days. The circles indicate precipitation amount, and squares represent the number of precipitation days.

focusing on the highest percentile. We found that the magnitude (precipitation per day) of stations above 1 km exhibit a power-law relation with generally decreasing power-law exponents with elevation. Based on the station data, we suggest that high-elevation stations have relatively more low frequency and high-magnitude events than lower elevation stations. We emphasise that the percentile approach did not discern this finding, and we suggest that rare but high-magnitude events are an essential part of the hydrologic system that is best deciphered by long time series of rainfall station data.

Our empirical study of the variability of extreme precipitation in Nepal provides critical evidence on the potential risk of a hydrometeorological extreme event in the Nepalese Himalaya.

Declaration of competing interest

The authors declare that they have no known competing financial interests or personal relationships that could have appeared to influence the work reported in this paper.

CRediT authors contribution statement

Shakil Regmi: Conceptualisation, Software, Formal Analysis, Investigation, Resources, Data Curation, Writing—Original Draft Preparation, Project Administration, Funding Acquisition. Shakil Regmi and Bodo Bookhagen: Methodology, Validation, Writing—Review & Editing, Visualization. Bodo Bookhagen: Supervision.

Declaration of competing interest

The authors declare that they have no known competing financial interests or personal relationships that could have appeared to influence the work reported in this paper.

Acknowledgements

This research article is part of the corresponding author's PhD research project at Martin Luther University Halle—Wittenberg. Thus, the corresponding author thanks Martin Lindner for his supervision during this project. We also heartfully thank the two anonymous reviewers for their review and comments. The PhD project was funded by the Graduate Funding Commission of Martin Luther University Halle-Wittenberg under the Graduate Promotion Act of Saxony-Anhalt. The data acquisition from the Department of Hydrology and Meteorology of Nepal was funded by B. Bookhagen. We acknowledge the financial support from the South-Eastern Finland University of Applied Science's library for the open access publication of this article.

Appendix A. Supplementary data

Supplementary data to this article can be found online at https://doi.org/10.1016/j.wace.2022.100470.

References

Alviolo, M., Guzzetti, F., Rossi, M., 2014. Scaling properties of rainfall induced landslides predicted by a physically based model. Geomorphology 213, 38–47. https://doi.org/10.1016/j.geomorph.2013.12.039.

Andermann, C., Bonnet, S., Gloaguen, R., 2011. Evaluation of precipitation data sets along the Himalayan front. G-cubed 12 (7), Q07023. https://doi.org/10.1029/2011GC003513.

Anders, A.M., Roe, G.H., Haller, B., Montogomery, D.R., Finnegam, N.J., Putkonen, J., 2006. Spatial Patterns of Precipitation and Topography in the Himalayas, vol. 398. Geological Society of America, pp. 39–53. https://doi.org/10.1130/2006.2398(03. *Special Paper*.

Archer, D.R., Fowler, H.J., 2004. Spatial and temporal variations in precipitation in the Upper Indus Basin, global teleconnections and hydrological implications. Hydrol. Earth Syst. Sci. 8 (1), 47–61. https://doi.org/10.5194/hess-8-47-2004.

Arnold, B.C., 2015. Pareto distribution. In: Balakrishnan, N., Colton, T., Everitt, B., Piegorsch, W., Ruggeri, F., Teugels, J.L. (Eds.), Wiley StatsRef: Statistics Reference Online. https://doi.org/10.1002/9781118445112.stat01100.pub2.

Ashcroft, L., Karoly, D.J., Dowdy, A.J., 2019. Historical extreme rainfall events in southeastern Australia. Weather Clim. Extrem. 25, 100210 https://doi.org/10.1016/j.wace.2019.100210.

Baidya, S.K., Shrestha, M.L., Sheikh, M.M., 2008. Trend in daily climatic extremes of temperature and precipitation in Nepal. J. Hydrol. Meteorol. 5 (1), 38–51. Retrieved October 22, 2019, from. http://soham.org.np/wp-content/uploads/2008/03/v5-38-51.pdf.

Barros, A.P., 2004. On the Space-Time Patterns of Precipitation in the Himalayan Range: a Synthesis. *6th International GAME Conference*. Kyoto. Retrieved August 12, 2016, from. http://www.hyarc.nagoya-u.ac.jp/game/6thconf/html/abs_html/pdfs/T8APB19Oct04100318.pdf.

Barros, A.P., Lang, T.J., 2003. Monitoring the monsoon in the Himalayas: observations in Central Nepal, June 2001. Mon. Weather Rev. 131, 1408–1427. https://doi.org/10.1175/1520-0493 (2003)131<1408:MTMITH>2.0.CO;2.

Barros, A.P., Chiao, S., Lang, T.J., Burbank, D., Putkonen, J., 2006. From weather to climate—seasonal and interannual variability of storms and implications for erosion processes in the Himalaya. In: Willett, S.D., Hovius, N., Brandon, M.T., Fisher, D. (Eds.), Tectonics, Climate, and Landscape Evolution. Geological Society of America, pp. 17–38. https://doi.org/10.1130/2006.2398(02.

Barros, A.P., Joshi, M., Putkonen, J., Burbank, D.W., 2000. A study of the 1999 monsoon rainfall in a mountainous region in central Nepal using TRMM products and rain gauge observations. Geophys. Res. Lett. 27 (22), 3683–3686. https://doi.org/10.1029/2000GL011827.

Barros, A.P., Kim, G., Williams, E., Nesbitt, S.W., 2004. Probing orographic controls in the Himalayas during the monsoon using satellite imagery. Nat. Hazards Earth Syst. Sci. 4, 29–51. https://doi.org/10.5194/nhess-4-29-2004.

Bhandari, D., Uprety, M., Ghimire, G., Kumal, B., Pokharel, L., Khadka, P., 2018. Nepal flood 2017: wake up call for effective preparedness and response. In: Rugby, UK: Practical Action. Retrieved September 14, 2019, from. https://reliefweb.int/sites/reliefweb.int/files/resources/Nepal_Flood_2017_WEB.PDF.

Bohlinger, P., Sorteberg, A., 2018. A comprehensive view on trends in extreme precipitation in Nepal and their spatial distribution. Int. J. Climatol. 38 (4), 1833–1845. https://doi.org/10.1002/joc.5299.

Bookhagen, B., 2010. Appearance of extreme monsoonal rainfall events and their impact on erosion in the Himalaya. Geomatics, Nat. Hazards Risk 1 (1), 37–50. https://doi.org/10.1080/19475701003625737.

Bookhagen, B., Burbank, D.W., 2006. Topography, relief, and TRMM-derived rainfall variations along the Himalaya. Geophys. Res. Lett. 33, 1–5. https://doi.org/10.1029/2006GL026037.

Bookhagen, B., Burbank, D.W., 2010. Toward a complete Himalayan hydrological budget: spatiotemporal distribution of snowmelt and rainfall and their impact on river discharge. J. Geophys. Res.: Earth Surf. 115 (F3) https://doi.org/10.1029/2009JF001426.

Bookhagen, B., Thiede, R.C., Strecker, M.R., 2005. Abnormal monsoon years and their control on erosion and sediment flux in the high, arid northwest Himalaya. Earth Planet Sci. Lett. 231, 131–146. https://doi.org/10.1016/j.epsl.2004.11.014.

Burbank, D.W., Blythe, A.E., Putkonen, J., Pratt-Sitaula, B., Gabet, E., Oskin, M., Ojha, T. P., 2003. Decoupling of erosion and precipitation in the Himalayas. Nature 426, 652–655. https://doi.org/10.1038/nature02187.

Caine, N., 1980. The rainfall intensity-duration control of shallow landslides and debris flows. Geogr. Ann. 62 (1), 23–27. https://doi.org/10.2307/520449.

Cannon, F., Carvalho, L.M., Jones, C., Norris, J., Bookhagen, B., Kiladis, G.N., 2017. Effects of topographic smoothing on the simulation of winter precipitation in High Mountain Asia. J. Geophys. Res. Atmos. 122, 1456–1474. https://doi.org/10.1002/2016JD026038.

Chalise, S.R., Khanal, N.R., 2002. Recent extreme weather events in the Nepal Himalaya. The extreme of the extremes: extraordinary flood. Reykjavik: IADS 271, 141–146. Retrieved June 11, 2019, from. http://hydrologie.org/redbooks/a271/iahs_271_141.pdf.

Clauset, A., Shalizi, C.R., Newman, M.E., 2009. Power-law distributions in empirical data. Soc Ind Appl Math. 51 (4), 661–703. https://doi.org/10.1137/070710111.

Croitoru, A.E., Piticar, A., Burada, D.C., 2016. Changes in precipitation extremes in Romania. Quat. Int. 415, 325–335. https://doi.org/10.1016/j.quaint.2015.07.028.

Dahal, R.K., Hasagawa, S., 2008. Representative rainfall thresholds for landslides in the Nepal Himalaya. Geomorphology 100 (3–4), 429–443. https://doi.org/10.1016/j.geomorph.2008.01.014.

Dimri, A.P., 2012. Atmospheric water budget over the western Himalayas in a regional climate model. J. Earth Syst. Sci. 121 (4), 963–973. https://doi.org/10.1007/s12040-012-0204-8.

Dimri, A.P., Mohanty, U.C., Azadi, M., Rathore, L.S., 2006. Numerical study of western disturbances over western Himalayas using mesoscale model. Mausam 57 (4), 579–590. Retrieved November 17, 2018, from. https://metnet.imd.gov.in/mausamdocs/15742_F.pdf.

Ding, Y., Sikka, D.R., 2006. The Asian monsoon. In: Synoptic Systems and Weather. Springer, Berlin, pp. 131–201. https://doi.org/10.1007/3-540-37722-0_4.

Dulal, K.N., Takeuchi, K., Ishidaira, H., 2006. A framework for the analysis of uncertainty in the measurement of precipitation data: a case study for Nepal. Agric. Eng. Int. CIGR J. VIII. Retrieved from. https://hdl.handle.net/1813/10579.

Eriksson, M., Jianchu, X., Shrestha, A.B., Vaidya, R.A., Nepal, S., Sandstroem, K., 2009. The Changing Himalayas - Impact of Climate Change on Water Resources and Livelihoods in the Greater Himalayas. International Centre for Integrated Mountain Development, Kathmandu. Retrieved August 21, 2017, from. http://lib.icimod.org/record/26471/files/attachment_593.pdf.

Flohn, H., 1957. Large-scale aspects of the ""summer monsoon"" in south and East Asia. J Meteorology Soc Jpn. 75, 180–186. https://doi.org/10.2151/jmsj1923.35A.0_180.

Gabet, E.J., Burbank, D.W., Pratt-Sitaula, B., Putkonen, J., Bookhagen, B., 2008. Modern erosion rates in the high Himalayas of Nepal. Earth Planet Sci. Lett. 267, 482–494. https://doi.org/10.1016/j.epsl.2007.11.059.

Goswami, B.N., 2005. South Asian monsoon. In: Lau, W.K., Waliser, D.E. (Eds.), Intraseasonal Variability in the Atmosphere-Ocean Climate System. Springer, Berlin, pp. 19–61. https://doi.org/10.1007/3-540-27250-X_2.

Government of Nepal, 2019, July 30. Hour Assessment of Flood *July 2019*, p. 72. *Retrieved November 27, 2019*, from Reliefweb International: https://reliefweb.int/sites/reliefweb.int/files/resources/2019%20Flood%20Assessment%20Report%20v2.pdf.

Hannah, D.M., Kansakar, S.R., Gerrard, A.J., Rees, G., 2005. Flow regimes of Himalayan rivers of Nepal: nature and spatial patterns. J. Hydrol. 308, 18–32. https://doi.org/10.1016/j.jhydrol.2004.10.018.

Haylock, M.R., Goodess, C.M., 2004. Interannual variability of European extreme winter rainfall and links with mean large-scale circulation. Int. J. Climatol. 24 (6), 759–776. https://doi.org/10.1002/joc.1033.

IFRC, 2014. Emergency plan of action (EPoA) Nepal: floods and landslides. Kathmandu: Intern Fed Red Cross Red Crescent Soc. Retrieved February 13, 2017, from http://adore.ifrc.org/Download.aspx?FileId=62833.

Karki, R., Hasson, S., Schickhoff, U., Scholten, T., Bohner, J., 2017. Rising precipitation extremes across Nepal. Climate 4, 2–25. https://doi.org/10.3390/cli5010004.

Krishnamurthy, C.K., Lall, U., Kwon, H.H., 2009. Changing frequency and intensity of rainfall extremes over India from 1951 to 2003. J. Clim. 22 (18), 4737–4746. https://doi.org/10.1175/2009JCLI2896.1.

Liu, X.D., Dong, B.W., 2013. Influence of the Tibetan Plateau uplift on the Asian monsoon-arid environment evolution. Chin. Sci. Bull. 58 (34), 4277–4291. https://doi.org/10.1007/s11434-013-5987-8.

Malamud, B.D., Turcotte, D.L., 2006. The applicability of power-law frequency statistics to floods. J. Hydrol. 322 (1–4), 168–180. https://doi.org/10.1016/j.jhydrol.2005.02.032.

Malik, N., Bookhagen, B., Marwan, N., 2012. Analysis of spatial and temporal extreme monsoonal rainfall over South Asia using complex networks. Clim. Dynam. 39 (3–4), 971–987. https://doi.org/10.1007/s00382-011-1156-4.

Malik, N., Bookhagen, B., Mucha, P.J., 2016. Spatiotemporal patterns and trends of Indian monsoonal rainfall extremes. Geophys. Res. Lett. 43 https://doi.org/10.1002/2016GL067841.

Nandargi, S., Dhar, O.N., 2011. Extreme rainfall events over the Himalayas between 1871 and 2007. Hydrol. Sci. J. 56 (6), 930–945. https://doi.org/10.1080/02626667.2011.595373.

Nepal, S., 2016. Impacts of climate change on the hydrological regime of the Koshi river basin in the Himalayan region. J Hydro-environ Res. 10, 76–89. https://doi.org/10.1016/j.jher.2015.12.001.

Norris, J., Carvalho, L.M., Jones, C., Cannon, F., 2020. Warming and drying over the central Himalaya caused by an amplification of local mountain circulation. Clim Atmos Sci. 3 (1), 1–11. https://doi.org/10.1038/s41612-019-0105-5.

Olen, S.M., Bookhagen, B., Hoffmann, B., Sachse, D., Adhikari, D.P., Strecker, M.R., 2015. Understanding erosion rates in the Himalayan orogen: a case study from the Arun Valley. J. Geophys. Res.: Earth Surf. 120 (10), 2080–2102. https://doi.org/10.1002/2014JF003410.

Panday, P.K., Thibeault, J., Frey, K.E., 2015. Changing temperature and precipitation extremes in the Hindu Kush-Himalayan region: an analysis of CMIP3 and CMIP5 simulations and projections. Int. J. Climatol. 35 (10), 3058–3077. https://doi.org/10.1002/joc.4192.

Panthi, J., Dahal, P., Shrestha, M.L., Aryal, S., Krakauer, N.Y., Pradhanang, S.M., Karki, R., 2015. Spatial and temporal variability of rainfall in the Gandaki River basin of Nepal Himalaya. Climate 3 (1), 210–226. https://doi.org/10.3390/cli3010210.

Prakash, P., 2018. Study the 2013 flood damages and risk assessment in Kedarnath, Himalaya area using geoinformatic techniques. J. Geogr. Nat. Disasters 8 (1), 216. https://doi.org/10.4172/2167-0587.1000216.

Rahmani, V., Hutchinson, S.L., Harrington Jr., J.A., Hutchinson, J.M., 2016. Analysis of frequency and magnitude of extreme rainfall events with potential impacts on flooding: a case study from the central United States. Int. J. Climatol. 36 (10), 3578–3587. https://doi.org/10.1002/joc.4577.

Reddy, D.V., Kumar, D., Saha, D., Mandal, M.K., 2008. The 18 August 2008 Kosi river breach: an evaluation. Curr. Sci. 95 (12), 1668–1669. Retrieved September 27, 2018,

from. http://www.indiaenvironmentportal.org.in/files/The%2018%20August%202008%20Kosi%20river%20breach.pdf.
Reliefweb, 2019, July 11. Nepal: Floods and Landslides - *Jul 2019* from Reliefweb: https://reliefweb.int/disaster/fl-2019-000083-npl. (Accessed 2 December 2019).
Shatnawi, R., Althebyan, Q., 2013. An Empirical Study of the Effect of Power Law Distribution on the Interpretation of OO Metrics. ISRN Software Engineering, 198937. https://doi.org/10.1155/2013/198937.
Sheikh, M.M., Manzoor, N., Ashraf, J., Adnan, M., Collins, D., Hameed, S.L.S.M., 2014. Trends in extreme daily rainfall and temperature indices over South Asia. Int. J. Climatol. 35 (7), 1625–1637. https://doi.org/10.1002/joc.4081.
Shrestha, A.B., Aryal, R., 2011. Climate change in Nepal and its impact on Himalayan glaciers. Reg. Environ. Change 11, 65–77. https://doi.org/10.1007/s10113-010-0174-9.
Shrestha, A.B., Bajracharya, S.R., Sharma, A.R., Duo, C., Kulkarni, A., 2017. Observed trends and changes in daily temperature and precipitation extremes over the Koshi river basin 1975–2010. Int. J. Climatol. 37 (2), 1066–1083. https://doi.org/10.1002/joc.4761.
Shrestha, M.L., 2000. Interannual variation of summer monsoon rainfall over Nepal and its relation to Southern Oscillation Index. Meteorol. Atmos. Phys. 75, 21–28. https://doi.org/10.1007/s007030070012.
Singh, P., Kumar, N., 1997. Effect of orography on precipitation in the western Himalayan region. J. Hydrol. 199, 183–206. https://doi.org/10.1016/S0022-1694(96)03222-2.
Smith, T., Bookhagen, B., 2018. Changes in seasonal snow water equivalent distribution in High Mountain Asia (1987 to 2009). Sci. Adv. 4 (1), e1701550 https://doi.org/10.1126/sciadv.1701550.
Stolbova, V., Martin, P., Bookhagen, B., Marwann, N., Kurths, J., 2014. Topology and seasonal evolution of the network of extreme precipitation over the Indian subcontinent and Sri Lanka. Nonlinear Process Geophys. 21, 901–917. https://doi.org/10.5194/npg-21-901-2014.
Stolbova, V., Surovyatkina, E., Bookhagen, B., Kurths, J., 2016. Tipping elements of the Indian monsoon: prediction of onset and withdrawal. Geophys. Res. Lett. 43, 3982–3990. https://doi.org/10.1002/2016GL068392.
Subash, N., Gangwar, B., 2014. Statistical analysis of Indian rainfall and rice productivity anomalies over the last decades. Int. J. Climatol. 34 (7), 2378–2392. https://doi.org/10.1002/joc.3845.
Talchabhadel, R., Karki, R.C., Parajuli, B., 2016. Intercomparison of precipitation measured between automatic and manual precipitation gauge in Nepal. Measurement 106, 264–273. https://doi.org/10.1016/j.measurement.2016.06.047.
Tang, H., McGuire, L.A., Kean, J.W., Smith, J.B., 2020. The impact of sediment supply on the initiation and magnitude of runoff-generated debris flows. Geophys. Res. Lett. https://doi.org/10.1029/2020GL087643.
Thapa, K., Endreny, T.A., Ferguson, C.R., 2018. Atmospheric rivers carry nonmonsoon extreme precipitation into Nepal. J. Geophys. Res. Atmos. 123 (11), 5901–5912. https://doi.org/10.1029/2017JD027626.
Thiede, R.C., Bookhagen, B., Arrowsmith, J.R., Sobel, E.R., Strecker, M.R., 2004. Climate control on rapid exhumation along the southern Himalayan front. Earth Planet Sci. Lett. 222, 791–806. https://doi.org/10.1016/j.epsl.2004.03.015.
United Nations, 2019, July 13. Nepal: Monsoon Flooding. R*etrieved November 27, 2019*, from Reliefweb International: https://reliefweb.int/sites/reliefweb.int/files/resources/RCO_Monsoon%20Flash%20Update1_13072019.pdf.
USGS, 2012, October 1. EarthExplorer from. https://earthexplorer.usgs.gov/. (Accessed 14 November 2016).
Webster, P.J., 1986. The variable and interactive monsoon. In: Fein, Stephens (Eds.), Monsoons. John Wiley Company, pp. 269–330 from. https://ci.nii.ac.jp/naid/10006234015/#cit. (Accessed 26 June 2017).
Wheeldon, R., Counsell, S., 2003. Power law distributions in class relationships. In: 3rd IEEE International Conference in Source Code Analysis and Manipulation. IEEE, Amsterdam, pp. 45–54. https://doi.org/10.1109/SCAM.2003.1238030.
Wulf, H., Bookhagen, B., Scherler, D., 2010. Seasonal precipitation gradients and their impact on fluvial sediment flux in the Northwest Himalaya. Geomorphology 112 (1–2), 13–21. https://doi.org/10.1016/j.geomorph.2009.12.003.
Wulf, H., Bookhagen, B., Scherler, D., 2012. Climatic and geologic controls on suspended sediment flux in the Sutlej River Valley, western Himalaya. Hydrol. Earth Syst. Sci. 16, 2193–2217. https://doi.org/10.5194/hess-16-2193-2012.
Yatagai, A., Kamiguchi, K., Arakawa, O., Hamada, A., Yasutomi, N., Kitoh, A., 2012. Constructing a long-term daily gridded precipitation dataset for Asia based on a dense network of rain gauges. Bull. Am. Meteorol. Soc. 93 (9), 1401–1415. https://doi.org/10.1175/BAMS-D-11-00122.1.